Chapter 3

The Method of Lines

3.1 Introduction

Various numerical algorithms have been utilized for the analysis of waveguide structures, the Method of Lines (MOL) is one of them. The MOL has been applied to several types of planar longitudinally uniform waveguide problems. The MOL has been used to analyze single discontinuity [44, 45] and multiple discontinuities in optical waveguides [29, 36, 46, 47, 48, 49, 50]. It has also been applied to solve non-linear waveguide problems [51] as well as diffraction problem from waveguide ends [52]. This method has also been used to model 3-D problems [53, 54, 55] for both optical and microwave waveguides.

3.2 Principle of the Algorithm

When the MOL is applied to two dimensional structures, the wave equation is discretized in the transverse direction (the direction normal to the direction of propagation) and calculated analytically in the longitudinal direction [50].

Figure 3.1 shows a planar two-dimensional waveguide structure in which the interfaces of layers are parallel to the z-axis. Consequently, discretization will be applied along the the x-axis. This implies that the field will be calculated on lines that are equidistant from each other and parallel to the z-axis. The investigated structure is bounded by an electric wall where $E_y = 0$ or a magnetic wall where $H_y = 0$ as appropriate. The resulting difference equations are then decoupled and manipulated through algebraic transformation.

In some instances, it might be more advantageous to have non-equidistant discretization. An example of this is the case when the widths of the different layers of the structure exhibit extreme differences which results in increasing the number of lines and, consequently the associated computational time and memory requirements. In such cases, the distance between the lines (i-e. mesh size) is increased in regions where the field exhibits smaller variations and vice versa [56, 57].

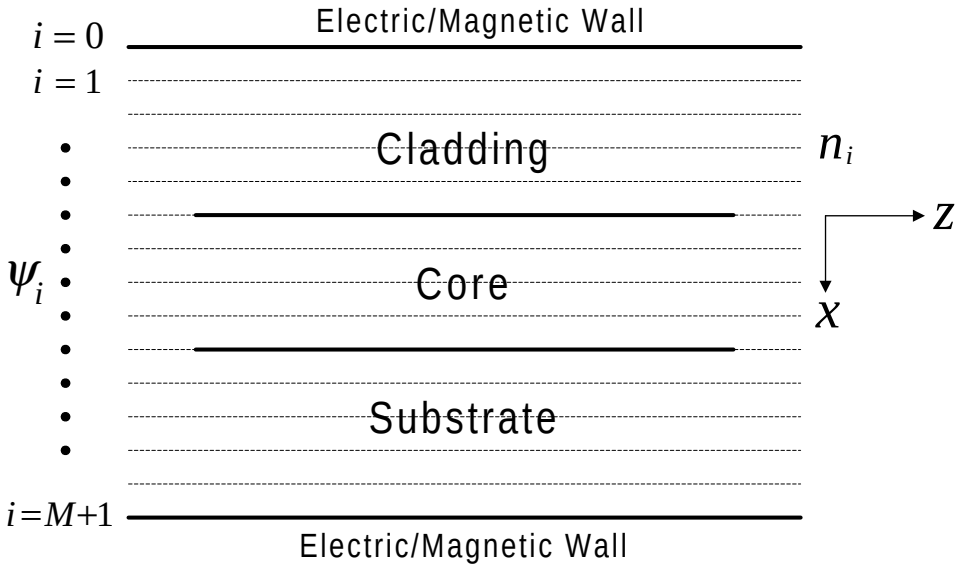

Figure 3.1: Mesh Discretization used in the MOL

3.3 Mathematical Formulation

Consider the two dimensional wave equation:

$$\frac{\partial^2\psi(x,z)}{\partial x^2} + \frac{\partial^2\psi(x,z)}{\partial z^2} + k_o^2 n^2 \psi(x,z) = 0 \tag{3.1}$$

where

ψ = Electric or Magnetic Field (E_y or H_y)

$k_o = 2\pi/\lambda_o$

λ_o = Free space wavelength

n = Refractive index of the medium

In the MOL, both the field $\psi(x,z)$ and the refractive index $n(x)$ are discretized along the x-axis and calculated on lines in the z-direction (direction of propagation). To calculate the field ψ in a discretized form, we first need to obtain its second derivative with respect to x in discrete form. This can be accomplished using the

well-known three-point central difference approximation.

3.3.1 The Three-Point Central Difference Approximation

To obtain an expression for the discretized second derivative of a certain function, we express the function in terms of a power series. We can have a good approximation of the given function in terms of a polynomial by neglecting all except the first few terms of the resulting series. One of the most convenient power series is the Taylor's Series which can be expressed as:

$$f(x) = \sum_{n=0}^{\infty} \frac{f^{(n)}(a)}{n!}(x-a)^n \tag{3.2}$$

where $f^{(n)}$ is the nth derivative of $f(x)$ with respect to x.

If Taylor's series is expanded about $x = 0$, the resulting series is often called a Maclaurin's Series expansion. Expanding $\psi(x)$ about $x = 0$ using equation 3.2:

$$\psi(x) = \psi(0) + \frac{\psi^{'}(0)}{1!}x + \frac{\psi^{''}(0)}{2!}x^2 + \frac{\psi^{'''}(0)}{3!}x^3 + \frac{\psi^{''''}(0)}{4!}x^4 + ... \tag{3.3}$$

Evaluating the above equation at $x = \pm\Delta x$ results in:

$$\psi_1 = \psi(0) + \frac{\psi^{'}(0)}{1!}\Delta x + \frac{\psi^{''}(0)}{2!}(\Delta x)^2 + \frac{\psi^{'''}(0)}{3!}(\Delta x)^3 + \frac{\psi^{''''}(0)}{4!}(\Delta x)^4 + ... \tag{3.4}$$

$$\psi_{-1} = \psi(0) - \frac{\psi^{'}(0)}{1!}\Delta x + \frac{\psi^{''}(0)}{2!}(\Delta x)^2 - \frac{\psi^{'''}(0)}{3!}(\Delta x)^3 + \frac{\psi^{''''}(0)}{4!}(\Delta x)^4 + ... \tag{3.5}$$

Adding equations 3.4 and 3.5, we have:

$$\psi_1 + \psi_{-1} = 2\psi(0) + \psi^{''}(0)(\Delta x)^2 + \frac{\psi^{''''}(0)}{12}(\Delta x)^4 + ... \tag{3.6}$$

this equation leads to:

$$\psi^{''}(0) = \frac{\psi_1 - 2\psi(0) + \psi_{-1}}{(\Delta x)^2} - \frac{\psi^{''''}(0)}{12}(\Delta x)^2 - ... \tag{3.7}$$

which can be approximated as:

$$\psi^{''}(0) \approx \frac{\psi_1 - 2\psi(0) + \psi_{-1}}{(\Delta x)^2} \tag{3.8}$$

It is apparent from equation 3.8 that the leading error resulting from the approximation is proportional to $(\Delta x)^2$.

3.3.2 Discretization of the Wave Equation

The second derivative operator ($\frac{\partial^2}{\partial x^2}$) term in equation 3.1 is replaced by the three-point central difference approximation from equation 3.8. So at the *ith* grid we get:

$$\frac{\psi_{i+1}(z) - 2\psi_i(z) + \psi_{i-1}(z)}{(\Delta x)^2} + \frac{d^2\psi_i(z)}{dz^2} + k_o^2 n_i^2 \psi_i(z) = 0 \tag{3.9}$$

If the field in the x-direction is discretized into M points, then equation 3.9 yields the following M equations:

$$i = 1: \qquad \frac{1}{(\Delta x)^2}\left[\psi_2 - 2\psi_1 + \psi_0\right] + \frac{d^2}{dz^2}\left[\psi_1\right] + k_o^2 n_1^2 \left[\psi_1\right] = 0 \tag{3.10}$$

$$i = 2: \qquad \frac{1}{(\Delta x)^2}\left[\psi_3 - 2\psi_2 + \psi_1\right] + \frac{d^2}{dz^2}\left[\psi_2\right] + k_o^2 n_2^2 \left[\psi_2\right] = 0 \tag{3.11}$$

$$i = 3: \qquad \frac{1}{(\Delta x)^2}\left[\psi_4 - 2\psi_3 + \psi_2\right] + \frac{d^2}{dz^2}\left[\psi_3\right] + k_o^2 n_3^2 \left[\psi_3\right] = 0 \tag{3.12}$$

$$\vdots$$

$$i = M: \qquad \frac{1}{(\Delta x)^2}\left[\psi_{M+1} - 2\psi_M + \psi_{M-1}\right] + \frac{d^2}{dz^2}\left[\psi_M\right] + k_o^2 n_M^2\left[\psi_M\right] = 0 \quad (3.13)$$

The above equations can be written in matrix form as:

$$\frac{1}{(\Delta x)^2}\begin{bmatrix} -2 & 1 & & & & & \\ 1 & -2 & 1 & & & \mathcal{O} & \\ & 1 & -2 & 1 & & & \\ & & \ddots & \ddots & \ddots & & \\ & \mathcal{O} & & & 1 & -2 & 1 \\ & & & & & 1 & -2 \end{bmatrix}\begin{bmatrix} \psi_1(z) \\ \psi_2(z) \\ \psi_3(z) \\ \vdots \\ \vdots \\ \psi_M(z) \end{bmatrix} + \frac{d^2}{dz^2}\begin{bmatrix} \psi_1(z) \\ \psi_2(z) \\ \psi_3(z) \\ \vdots \\ \vdots \\ \psi_M(z) \end{bmatrix}$$

$$+k_o^2\begin{bmatrix} n_1^2 & & & & & & \\ & n_2^2 & & & & \mathcal{O} & \\ & & n_3^2 & & & & \\ & & & \ddots & & & \\ & \mathcal{O} & & & \ddots & & \\ & & & & & & n_M^2 \end{bmatrix}\begin{bmatrix} \psi_1(z) \\ \psi_2(z) \\ \psi_3(z) \\ \vdots \\ \vdots \\ \psi_M(z) \end{bmatrix} = \begin{bmatrix} 0 \\ 0 \\ 0 \\ \vdots \\ \vdots \\ 0 \end{bmatrix}$$

written in compact notation, we get:

$$\frac{1}{(\Delta x)^2} C\Psi + \frac{d^2}{dz^2}\Psi + k_o^2 N\Psi = 0 \quad (3.14)$$

where C is a tri-diagonal second-order central-difference matrix , N is a diagonal matrix whose elements are $n_1^2, n_2^2, ..., n_M^2$ and $\Psi = [\psi_1(z), \psi_2(z), ..., \psi_M(z)]^t$ is the

discretized field vector of either E_y or H_y depending upon the polarization. The above equation may then be written in the form:

$$\frac{d^2}{dz^2}\Psi + Q\Psi = 0 \tag{3.15}$$

where

$$Q = \frac{1}{(\Delta x)^2}C + k_o^2 N \tag{3.16}$$

The solution of this 2nd-order ordinary matrix differential equation is formally given by [29]:

$$\Psi = e^{j\sqrt{Q}z}A + e^{-j\sqrt{Q}z}B \tag{3.17}$$

where $e^{j\sqrt{Q}z}$ represents field propagation in the $+z$ direction and $e^{-j\sqrt{Q}z}$ represents field propagation in $-z$ direction. The matrices $e^{j\sqrt{Q}z}$ and $e^{-j\sqrt{Q}z}$ are calculated by diagonalizing matrix Q to find the eigenvalues and eigenvectors. Matrix Q may be written in the form:

$$Q = UVU^{-1} \tag{3.18}$$

where U is the eigenvector matrix and V is a diagonal matrix containing the eigenvalues of Q. The matrix exponent is then calculated using the following well known relation of linear algebra:

$$e^{j\sqrt{Q}z} = Ue^{j\sqrt{V}z}U^{-1} \tag{3.19}$$

3.4 Convergence of the MOL

The convergence behavior of the results of a numerical method serves as a good indicator of the accuracy of the chosen parameters. One important parameter in the MOL is the mesh size (h) that is the number of discretization lines (M). The accuracy of the results should improve as the mesh size decreases. However, as mesh size decreases, the number of discretization lines increases. This leads to longer computational time and larger memory requirement.

3.5 Interface Conditions

In order to correctly model the electric and magnetic fields behavior at an interface, the interface conditions (I.Cs.) should be appropriately accounted for in the Method of Lines formulation. In this thesis, we are mainly concerned with multi-layer structures in which the material properties are constant within each layer and change abruptly from one layer to the next (see figure 2.2). The tangential electric field E_y and its first derivative are continuous across an interface. The tangential magnetic field H_y is continuous but its first derivative is discontinuous at an interface. All the higher order derivatives of both E_y and H_y are discontinuous at an interface. We can derive these relations using Maxwell equations. For TE polarization, applying equation 2.19

$$H_z = -\frac{j}{\omega \mu_o} \frac{\partial E_y}{\partial x} \tag{3.20}$$

at an interface along with the fact that H_z is continuous at an interface, that is $H_z^{0^+} = H_z^{0^-}$, equation 3.20 gives:

$$-\frac{j}{\omega\mu_o}\frac{\partial E_y^{0^+}}{\partial x} = -\frac{j}{\omega\mu_o}\frac{\partial E_y^{0^-}}{\partial x} \tag{3.21}$$

that is

$$\frac{\partial E_y^{0^+}}{\partial x} = \frac{\partial E_y^{0^-}}{\partial x} \tag{3.22}$$

which is the statement of the continuity of $\frac{\partial E_y}{\partial x}$ at a horizontal interface. Similarly for TM polarization, using equation 2.30

$$E_z = \frac{j}{\omega n_j^2 \epsilon_o}\frac{\partial H_y}{\partial x} \tag{3.23}$$

at an interface along with the fact that E_z is continuous, that is $E_z^{0^+} = E_z^{0^-}$, we obtain:

$$\frac{j}{\omega n_2^2 \epsilon_o}\frac{\partial H_y^{0^+}}{\partial x} = \frac{j}{\omega n_1^2 \epsilon_o}\frac{\partial H_y^{0^-}}{\partial x} \tag{3.24}$$

that is:

$$\frac{1}{n_2^2}\frac{\partial H_y^{0^+}}{\partial x} = \frac{1}{n_1^2}\frac{\partial H_y^{0^-}}{\partial x} \tag{3.25}$$

which means that $\frac{\partial H_y}{\partial x}$ is discontinuous at a horizontal interface.

Depending upon the polarization of the field, ψ may represent either E_y for the TE polarization or H_y for the TM polarization. At an index discontinuity in the transverse direction x, ψ is continuous. However, all its higher order derivatives with respect to x are in general discontinuous there. With reference to Figure 3.2,

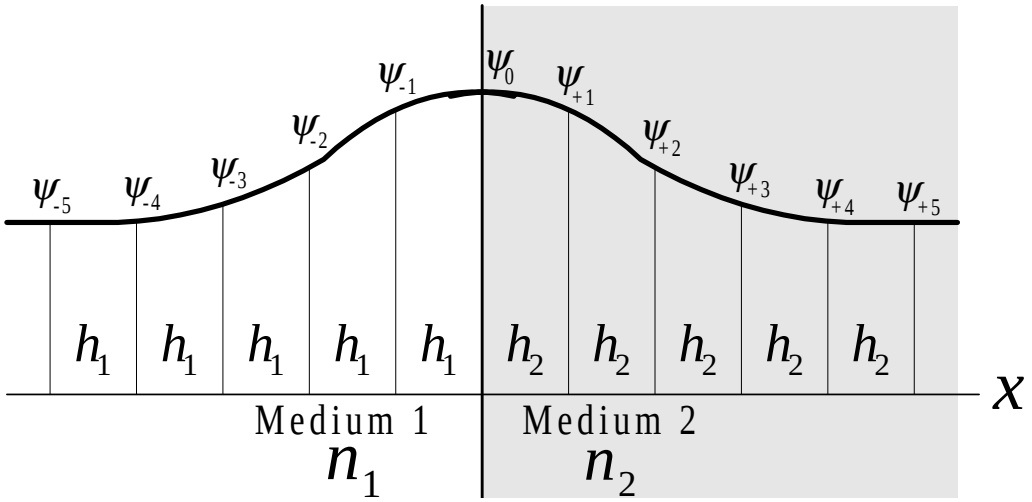

Figure 3.2: Discretized Field in the Transverse Direction

where an index discontinuity is assumed to exist at $x = 0$, the discontinuities in the higher-order derivatives of ψ can easily be deduced from the wave equation, and are summarized below [58]:

$$\psi_{0+} = \psi_{0-} = \psi_0 \tag{3.26}$$

$$\psi'_{0+} = \rho_{21}\psi'_{0-} \tag{3.27}$$

$$\psi''_{0+} = \psi''_{0-} + \zeta_{12}\psi_0 \tag{3.28}$$

$$\psi'''_{0+} = \rho_{21}\left(\psi'''_{0-} + \zeta_{12}\psi'_{0-}\right) \tag{3.29}$$

$$\psi''''_{0+} = \psi''''_{0-} + 2\zeta_{12}\psi''_{0-} + \zeta_{12}^2\psi_0 \tag{3.30}$$

$$\psi'''''_{0+} = \rho_{21}\left(\psi'''''_{0-} + 2\zeta_{12}\psi'''_{0-} + \zeta_{12}^2\psi'_{0-}\right) \tag{3.31}$$

$$\psi''''''_{0+} = \psi''''''_{0-} + 3\zeta_{12}\psi''''_{0-} + 3\zeta_{12}^2\psi''_{0-} + \zeta_{12}^3\psi_0 \tag{3.32}$$

where $\zeta_{12} = k_o^2(n_1^2 - n_2^2)$, $\rho_{21} = n_2^2/n_1^2$ for the TM case and $\rho_{21} = 1$ for the TE case.

The subscripts 0^+ and 0^- represent the field immediately to the right and to the left of the interface, respectively.

3.6 Improved Three-Point Formulation with Interface Conditions

The field is sampled or discretized so that there is always a sample point at an interface. Within a certain layer i, the refractive index n_i and mesh size h_i are uniform. From one layer to the next, either the refractive index n_i or the mesh size h_i or both may abruptly change. The refractive index chosen at the interface sampling point is either the refractive index of left layer or the refractive index of right layer. This choice should be consistent throughout the whole structure. In this manner, we can correctly model the layer thickness and abrupt refractive index discontinuity. With reference to figure 3.2, the field on either side of the interface is expanded in terms of the field at the interface using Taylor's series expansion, that is:

$$\psi_{-1} = \psi_{0^-} - h_1\psi'_{0^-} + \frac{h_1^2}{2!}\psi''_{0^-} + ... \tag{3.33}$$

$$\psi_{+1} = \psi_{0^+} + h_2\psi'_{0^+} + \frac{h_2^2}{2!}\psi''_{0^+} + ... \tag{3.34}$$

Here ψ_{0^+} and ψ_{0^-} represent the field at $x = 0^+$ and $x = 0^-$ respectively. Using the interface conditions 3.26, 3.27 and 3.28 and expressing all ψ_{0^+} in terms of ψ_{0^-}

in equation 3.34, we obtain:

$$\psi_{+1} = \left(1 + 0.5h_2^2\zeta_{12}\right)\psi_o + h_2\rho_{21}\psi_{0-}^{'} + 0.5h_2^2\psi_{0-}^{''} + ... \tag{3.35}$$

Eliminating $\psi_{0-}^{'}$ from equations 3.35 and 3.33, we get [36, 58]:

$$\psi_{0-}^{''} = \frac{\psi_{+1} - (\tau_{21}\rho_{21} + 1 + 0.5h_2^2\zeta_{12})\,\psi_0 + \tau_{21}\rho_{21}\psi_{-1}}{0.5h_2(h_1\rho_{21} + h_2)} \tag{3.36}$$

where $\tau_{21} = \frac{h_2}{h_1}$. The above relation can be used to approximate the $\frac{\partial^2}{\partial x^2}$ operator at any sampling point i in terms of the field values at $i+1$, i and $i-1$ sampling points. So this represents an improved three-point finite-difference approximation of $\frac{\partial^2}{\partial x^2}$ operator because it accounts for the interface boundary conditions. In the case of uniform refractive index and uniform mesh size i.e. $n_1 = n_2$ and $h_1 = h_2$, equation 3.36 reduces to the familiar three-point central-difference approximation, that is:

$$\psi_{0-}^{''} \approx \frac{\psi_{+1} - 2\psi_0 + \psi_{-1}}{h^2} \tag{3.37}$$

3.7 Higher-Order Finite Difference Approximation

The improved formula 3.36 for the second derivative approximation has an accuracy of $O(h^2)$ at regions of uniform index and mesh size. Its accuracy decreases at a mesh or index discontinuity. In integrated optical waveguide modeling, the required accuracy in estimating the effective index is fairly high. So we need to use a relatively

large number of discretization lines to reduce numerical errors. This leads to larger matrices and longer computational time.

The higher-order approximation scheme of the second-derivative operator $\frac{\partial^2}{\partial x^2}$ presented in references [36, 58] gives sufficiently high accuracy and accurate estimation of the modal field profile and the effective indices. The necessary interface conditions for the electric and magnetic fields are appropriately included in the scheme. This scheme results in a much reduced matrix size, faster computational speed and lower memory usage. This high-order approximation scheme is discussed in appendix A and it is used in this thesis.

3.8 Results

The previously developed formulae for the three-point, five-point and seven-point approximation of the second derivative operator ($\frac{\partial^2}{\partial x^2}$) are used to model a high-contrast waveguide and a metal-dielectric single interface. The effective index n_{eff} and modal field of the fundamental TE and TM modes are calculated using the MOL. These MOL results are compared with exact results and their convergence behavior is studied by decreasing the mesh size (that is increasing the number of discretization points) in the problem space. It is observed that the 7-point formula gives a better estimate of n_{eff} and modal field with relatively few sample points as compared to the 5-point and the 3-point formulas. The basic 3-point formula without interface conditions can not distinguish between the TE and TM polarizations.

3.8.1 High-Contrast Waveguide

A high-contrast waveguide structure (shown in the inset of figure 3.3) is modeled using the MOL. In this simulation, a uniform mesh is used and the mesh size is varied. During simulation the outermost layers thickness is kept sufficiently large so that the modal field decays to a sufficiently small value (approximately 10^{-5}) as compared to its value at the $Air/GaAs$ interface. The phase parameter, defined as $B = (n_{eff}^2 - 1^2)/(3.6^2 - 1^2)$, is used to assess the accuracy of the computed results. The exact values of the TE_0 and TM_0 modes are calculated by STF1 program (see Appendix B). For the TE_0 mode, we have $n_{eff} = 3.543961609340564$ and $B_0 = 0.9665270809765686$, and for the TM_0 mode, $n_{eff} = 3.529434420038923$ and $B_0 = 0.9579353950966126$. The relative error in phase parameter which is defined as $\frac{B_{MOL} - B_0}{B_0}$ is plotted against the mesh size (h) (see figures 3.3 and 3.4). The results show that for relatively large values of the mesh size, the error due to higher order formulation exceeds the corresponding error for lower order formulation. However, as the mesh size decreases, the error due to higher order formulation becomes much lower than that due to the lower order formulation [58]. This shows the superiority of the 5-point and the 7-point formulation to find n_{eff} and modal field for both the TE and TM polarization as compared to the 3-point formulation.

The 7-point formulation takes approximately 0.10 seconds per mesh size to calculate the relative error in the phase parameter for TE_0 mode and the 3-point and 5-point formulation take 0.02 and 0.08 seconds per mesh size respectively (using an

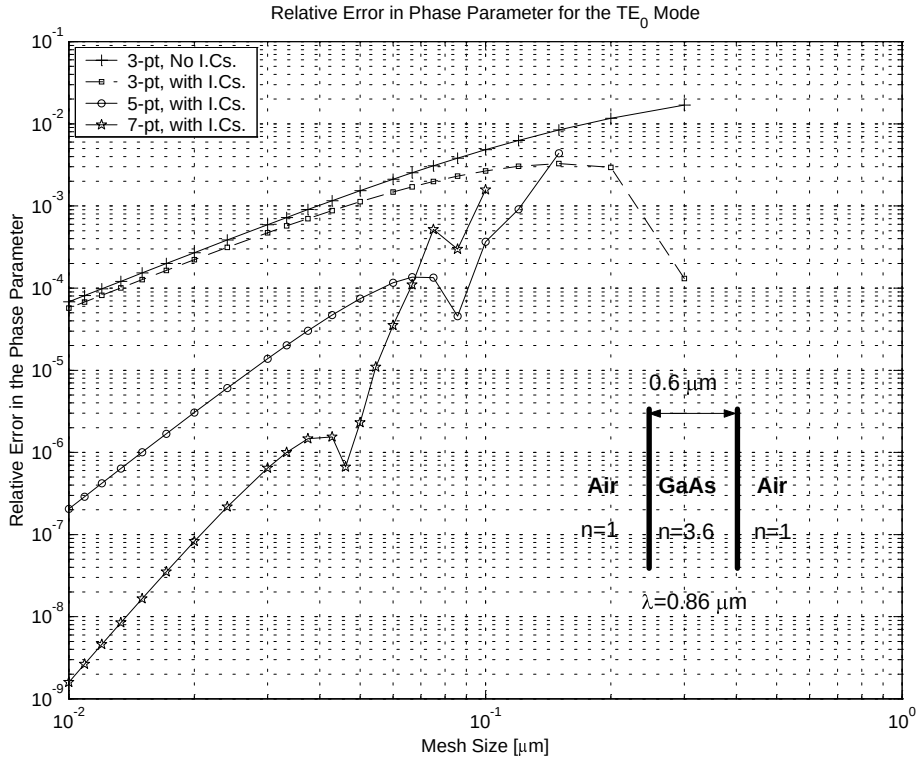

Figure 3.3: Relative Error in Phase Parameter for the TE_0 Mode

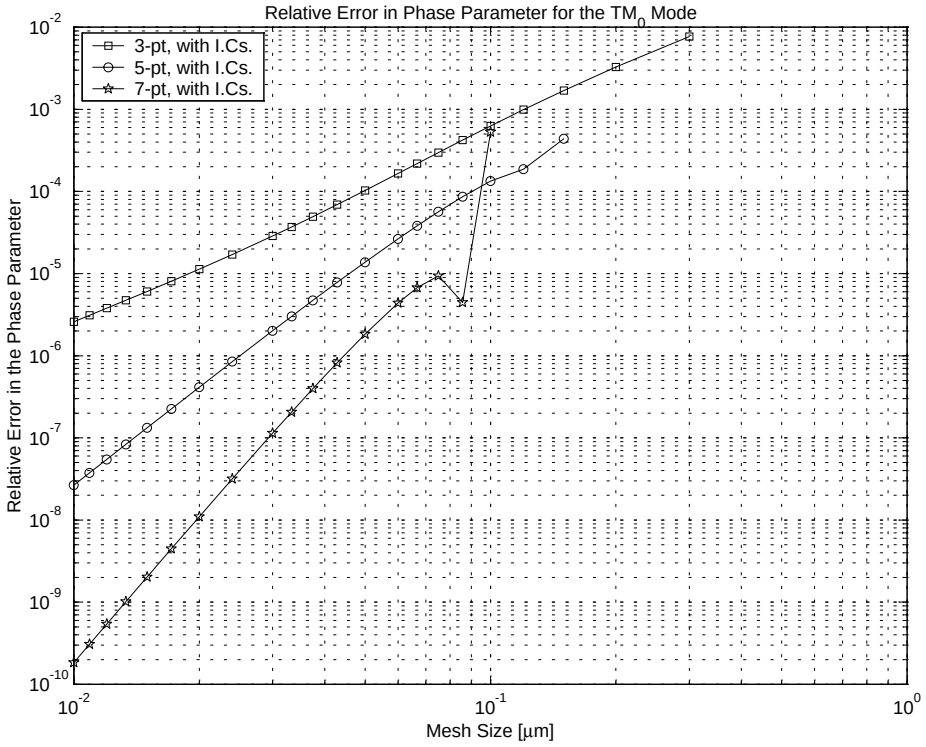

Figure 3.4: Relative Error in Phase Parameter for the TM_0 Mode

IBM Pentium-III machine with 128 MB RAM running MATLAB 5.2 under Windows 98). This indicates that the 5-point and 7-point formulation are slow as compared to the 3-point formulation.

3.8.2 Metal-Dielectric Single Interface

The single interface between a metal and a dielectric supports a surface plasmon mode. This mode is TM polarized and is characterized by a field (called evanescent field) that decays exponentially on both sides of the interface. This field decays in the metal much faster than it does in air. A Surface plasmon mode is known to be lossy with a complex propagation constant [39, 59]. It can only exist as surface wave at a metal/dielectric interface when the complex dielectric constant (i-e. n^2) of the metal has a negative real part. The following analytic expression is used to calculate the effective index (n_{eff}) of the surface plasmon mode [58].

$$n_{eff} = \frac{n_1 n_2}{\sqrt{n_1^2 + n_2^2}} \tag{3.38}$$

where n_1 and n_2 are the refractive indices of the metal and dielectric respectively.

A metal/air single interface structure (see figure 3.5) is modeled at the operating wavelength, $\lambda = 0.6328\mu m$. The problem space is divided into many artificial layers and a non-uniform discretization scheme is used to sample the waveguide efficiently. A fine mesh is used in regions of fast field decay and a coarse mesh is employed in regions of slow field decay. This decreases the total number of sampling points considerably as compared to a uniform sampling scheme. The effective index is

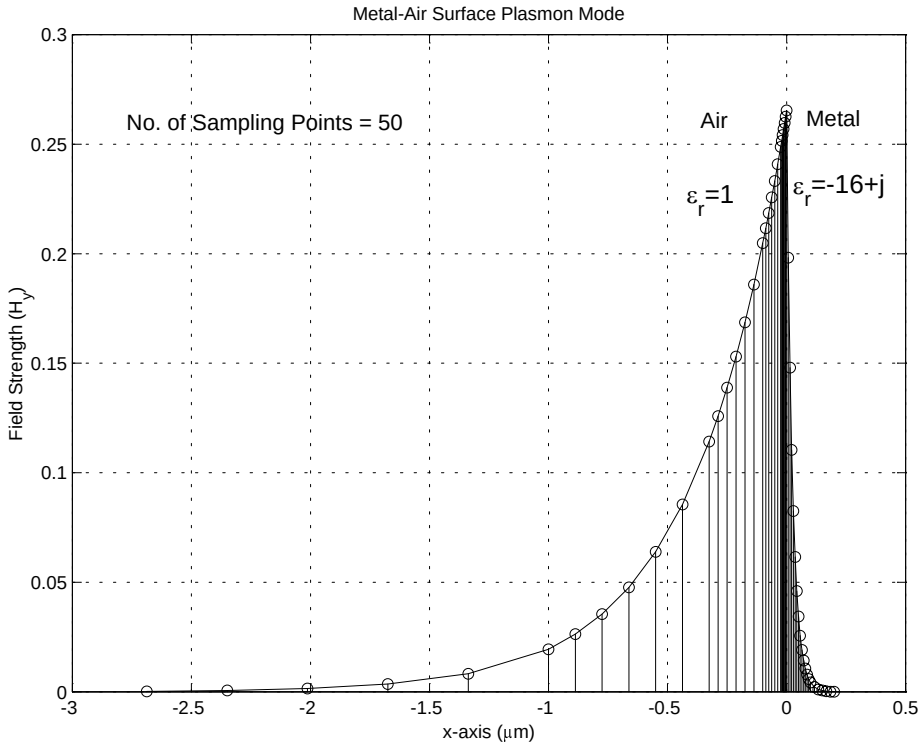

Figure 3.5: Magnetic Field Pattern of A Surface Plasmon Mode at a Metal-Air Interface

calculated and compared against analytical values for the 3-point, the 5-point and the 7-point formulations. The results are given in table 3.1. It is found that the 7-point formulation gives more accurate results than the 5-point or the 3-point schemes for a fixed total number of mesh points [58]. The basic 3-point formulation without interface conditions can not be used to model this problem. The results obtained are in close agreement with those given in reference [36].

3-Point	5-Point	7-Point
-5.046e-4+j7.733e-6	7.652e-6-j8.145e-7	1.147e-8+j3.261e-8

Table 3.1: Error in n_{eff} for the Surface Plasmon Mode. (Analytical value of $n_{eff} = 1.032654962422412 + j0.002142428459687181$, total number of sampling points = 50)